Analysis of patterns in the concentrations of atmospheric greenhouse gases measured in two typical urban clusters in China

Lixin Liu[a, b *], Pieter P. Tans[c], Lingjun Xia[d], Lingxi Zhou[b], Fang Zhang[e]

a China Meteorological Administration Meteorological Observation Centre (CMA-MOC), Beijing 100081, China
b Chinese Academy of Meteorological Sciences (CAMS), China Meteorological Administration (CMA), Beijing 100081, China
c Climate Monitoring and Diagnostics Laboratory, National Oceanic and Atmospheric Administration, Boulder, Colorado 80305, USA
d Jiangxi Climate Center, Nanchang 330096, China
e College of Global Change and Earth System Science, Beijing Normal University, Beijing 100875, China

Correspondence to: Lixin Liu (liulx@camscma.cn)

Highlights

- Background values at SDZ were mainly influenced by long-distance transportation.
- Background values at LAN are obviously higher than other stations.
- Polluted data at SDZ and LAN are strongly affected by regional and local emissions.
- Polluted CO_2 concentration at LAN is lower than that at SDZ in autumn and winter.
- Coal and biomass burning in JJJ lead to the higher ratios of ΔCO_2-ΔCO at SDZ.

Keywords

greenhouse gases; regional influence; urban clusters; back-trajectory cluster analysis; correlation analysis

Abstract

China is the largest emitter of greenhouse gases, and urban clusters play an essential role in China's carbon emissions because of the country's unbalanced economic development. In

this paper, the discrete air sample measurements of atmospheric CO_2, CH_4, and CO during the period between 2007 and 2013 from Shangdianzi (SDZ) station in Jing-Jin-Ji (JJJ) region and Linan (LAN) station in Yangtze River Delta (YRD) region, respectively, are presented and characterized. By backward trajectory cluster analysis, the low background CO_2 mole fraction and similar long-term trends with Waliguan global station (WLG) were observed at SDZ because most of the air masses originate mostly from remote clean terrestrial areas in the north with limited information of anthropogenic emissions. But the background CH_4 and CO are influenced mainly by ruminants and rice field emission from the surrounding regions and urban cluster emission in the JJJ region, which lead to the higher CH_4 and CO in summer at SDZ. Whereas, the CO_2, CH_4 and CO background values observed at LAN are higher by the combined effects of long-distance atmospheric transportation from Northern and Central China and urban clusters emission from the YRD region. The observed polluted data at SDZ and LAN are all strongly affected by regional and local anthropogenic emissions, which lead to the higher GHGs concentrations compared to the background data. However, because the air mass transportation from the north is weak in winter and no winter heating is required and vegetation photosynthesis is still stronger in the south of China, the CO_2 concentration at LAN is lower than that at SDZ in autumn and winter. The polluted CO value at SDZ is found considerably higher than that at LAN, especially in spring and winter. By analyzing the correlations of observed regional enhanced values of CO_2, CH_4 and CO at the two stations, we find the significant correlation between them, which means they may share the common-source of anthropogenic emissions from the regional fossil fuel and biomass burning in cold season. Moreover, the high coal-consumption proportion with the low CO_2 emissions factors, and much biomass burning with low combustion efficiency in JJJ region lead to the higher slope values of $\triangle CO_2$ and $\triangle CO$ in spring and winter at SDZ and considerably higher than that at LAN. The results can provide a further understanding of regional/local features of atmospheric GHGs under the influence of human activities in the urban clusters in China.

1. Introduction

Carbon dioxide (CO_2) and methane (CH_4) are the two most important anthropogenic greenhouse gases (GHGs) in the atmosphere. These gases contribute approximately 65% and 17% of total radiative forcing from long-lived greenhouse gases, respectively. Global atmospheric CO_2 concentrations reached 143% of pre-industrial level in 2014, primarily because of emissions from the combustion of fossil fuels (90%) and cement production (10%). Atmospheric CH_4 reached 254% of its pre-industrial level in 2014 (Liu, 2015; WDCGG, 2014; WMO, 2015). CH_4 is driven mainly by reaction with hydroxyl radical (OH) and emissions from sources such as wetlands, fossil fuel and biomass burning, as well as by atmospheric transport. Carbon monoxide (CO) is not a greenhouse gas, but its most prominent sources are closely associated with primary emissions from the incomplete combustion of fossil fuels and biomass. Therefore, CO is a good indicator of anthropogenic pollution (Gamnitzer et al., 2006; Levin and Karstens, 2007; Turnbull et al., 2006).

China, with its fast-growing economy, is the largest emitter of GHGs (Boden et al., 2010; Gregg et al., 2008). However, the characteristics and the level of GHGs emissions vary among different regions. Cities play an essential role in China's carbon emissions; more specifically, 85% of China's direct carbon emissions are from cities (Liu, 2015). Therefore, observing atmospheric CO_2 and CH_4 concentrations in combination with the characteristics of the natural and socio-economic environment in different regions can yield important information on regional GHGs sources and sinks.

Previous studies have mostly focused on long-term observations of atmospheric greenhouse gases and related gases from Waliguan (WLG) global background station (Zhang et al., 2011, 2013a, 2013b; Zhou et al., 2004a, 2004b, 2005). Few studies have been published based on the observations from regional stations because of insufficient data and the complex distribution of multiple sources and sinks, especially in the economically developed urban areas (Fang et al., 2013, 2014; Liu et al., 2009, 2014; Pu et al., 2014).

The Jing-Jin-Ji region (JJJ region) encompasses Beijing and Tianjin, as well as eight other cities and more than 80 counties in Hebei province (Fig. 1), is located in the North China Plain. This region is the political center of China and the most important economic center in northern China. The rate of economic growth in this area is well above the national average, but the pattern of development, which has focused on heavy

industry, has increasingly caused prominent environmental and resource problems (Feng et al., 2013; Han et al., 2009; Wang et al., 2014). On the other hand, the Yangtze River Delta region (YRD region), which lies on the eastern coast of China, includes Shanghai, Jiangsu province, and Zhejiang province. This region has the fastest growing regional economy, making the largest contribution to the Chinese economy, and has the highest urbanization rate and the largest foreign trade base in China (Sun et al., 2012; Wu et al., 2012).

In terms of emissions of GHGs and pollutants, these two urban clusters are the most important regions because of the positive association between anthropogenic emissions and recent rapid economic growth (Deng et al., 2014; Du and Fan, 2008; Long et al., 2015). In June 2006, the greenhouse gases and related tracers laboratory of the CMA began measuring GHGs from flask samples collected at Shangdianzi station (SDZ), which is located in the JJJ region, and Lin'an station (LAN), which is located in the YRD region. Both stations are regional stations of the World Metrological Organization (WMO) / Global Atmosphere Watch (GAW) (Zhou et al., 2008).

In this paper, the discrete air sample measurements of atmospheric CO_2, CH_4, and CO from stations SDZ and LAN are presented and characterized. The study periods are from January 2007 to December 2013 for CO_2 and CH_4 and from October 2008 to December 2013 for CO from both stations. The temporal variations and regional background characters are introduced and are compared with GHGs data results recorded at other observational stations. The regional/local impacts of high anthropogenic emissions in urban clusters on the observed GHGs mixing ratios have been mainly investigated by trajectory cluster analysis and correlation analysis of enhanced CO_2, CH_4 and CO values.

2. Sites and Experimental Methods

2.1 Sites description

Fig. 1 shows the locations of SDZ, LAN and major cities. SDZ (40°39'N, 117°07'E, 293 m asl) is located within the JJJ region in the North China Plain, 100 km northeast of urban Beijing. The main weather systems there with a temperate continental monsoon climate, are affected by the region of strong high pressure over Mongolia in winter and the region of

low pressure over India in summer. LAN (30°18'N, 119°44'E, 139 m asl) is located in the center of the YRD region, 40 km west and 150 km southwest of the major population centers of Hangzhou and Shanghai, respectively. The dominant wind direction is affected by the Siberian cold current in winter and the temperature contrast between the land and sea in summer.

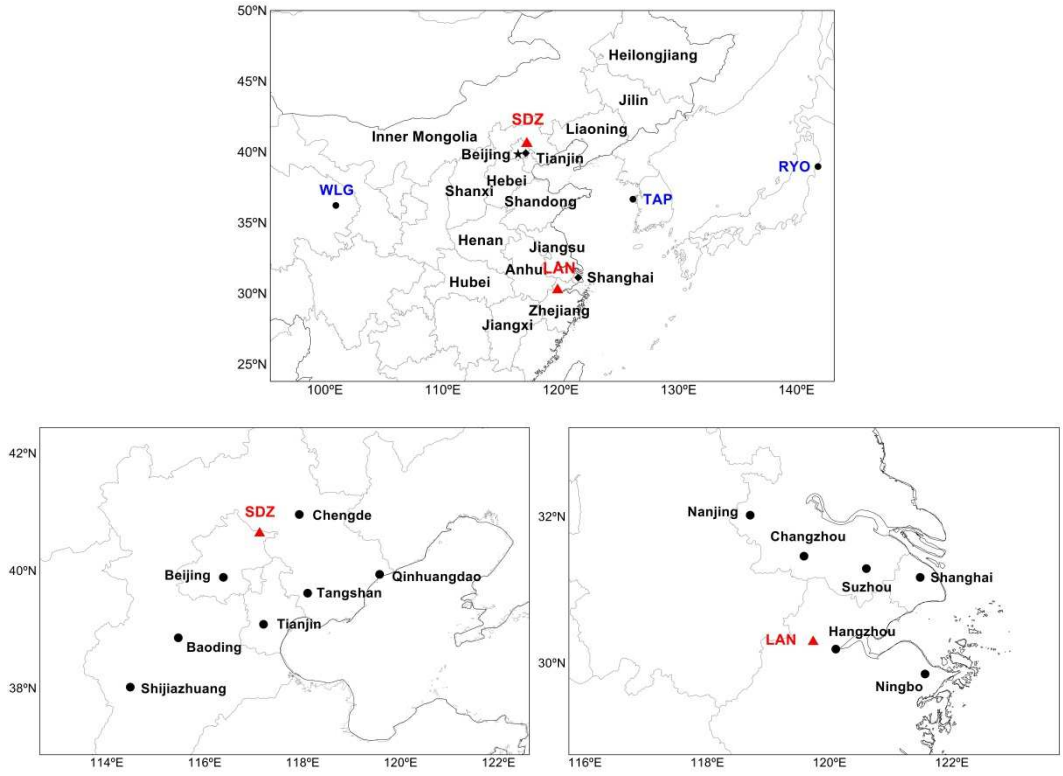

Fig. 1. Map of study region, showing the locations of SDZ and LAN stations (red triangles), main provinces and cities. (The areas are 218331 km^2, 213018 km^2, and the population densities are 4.93, 7.41 10^3/km^2 in JJJ and YRD, respectively.)

2.2 Experimental methods

This study is based on discrete air sample measurements. Both the sampling and analyses were conducted using methods recommended by WMO/GAW (Trolier et al., 1996; WMO, 2009, 2011). The sampling equipment consisted of a portable pumping unit (HPD, Sherpa 60) and 2.2 L Pyrex glass flasks with two stopcocks that are made according to the specifications of the National Oceanic and Atmospheric Administration (NOAA) Earth System Research Laboratory and allow complete sample flushing prior to capture (Lang et al., 1994). The flask samples were collected weekly in pairs during the early to mid-afternoon,

when vertical atmospheric mixing was most vigorous. Before sampling, all flasks were subjected to a vacuum test in the laboratory to detect and avoid gas leakage. Subsequently, they were filled with dry balance gas at a pressure slightly higher than atmospheric pressure to condition the internal surfaces of the flasks. Sampling was delayed if the wind speed decreased to below 2 m/s or when atmospheric conditions became rainy, foggy, or dusty (Liu et al. 2009, 2014).

Prior to October 2009, the CO_2 mole fraction was measured with a non-dispersive infrared analyzer system (LI-7000, Li-cor, USA), and subsequently with a Picarro G-1301 unit, whose principle of operation is based on cavity ring down spectroscopy (CRDS). CH_4 and CO mole fractions were measured with a Gas Chromatography-Flame Ionization Detector (GC-FID) system (6890N, Agilent Technologies, USA). The samples were calibrated using a linear two-point fit for CRDS and GC-FID, with one working standard at a high concentration and the other at a low concentration (Liu et al., 2014; Zang et al., 2011; Fang et al., 2014). For NDIR, a curve was fitted to five calibration points over a wider range to calibrate the instrument (Zhang et al., 2005). The standard gases used in measuring CO_2, CH_4 and CO mole fractions are directly traceable to the WMO-CO_2-X2007 scale, the WMO-CH_4-X2004A scale and the WMO-CO-X2014 scale maintained by NOAA (Zhao et al., 1997; http://www.esrl.noaa.gov/gmd/ccl/). In addition, a calibrated cylinder filled with compressed ambient air was used as a target gas (T) to check the precision and stability of the system, and no evidence of drift was observed during the whole study period. The analytical precision and stability of CO_2 are 0.06ppm and 0.05ppm by LICOR, while CH_4 has 0.3ppb and 0.4ppb by CRDS, and CO has 2ppb and 1ppb by GC, respectively. The observed quality meets the requirements of recommended compatibility of measurements within the scope of WMO/GAW during each spot supervision and assessment by WMO/WCC (World Calibration Centre) (https://gaw.kishou.go.jp/wcc/ch4/com_annex2.html) and Round-Robin every 2-3 years (Zhou, 2009; https://www.esrl.noaa.gov/gmd/ccgg/wmorr/wmorr_status.php).

2.3 Data processing methods

Based on the observed data from weekly flask sampling, some of the data, which was

potentially affected by improper operations during sampling, e.g., sampling under poor weather conditions (as judged from the sampling information record), or instrument fluctuations in analysis (as judged from T based on the threshold value of 0.2 ppm, 5 ppb and 5 ppb for CO_2, CH_4 and CO, respectively), were rejected (WMO, 2011). Then, because the GHGs concentration variation are a seasonal change and a long-term trend by removing local effects with very-short-term variation, in this paper, they were derived by curve-fitting and digital filtering recommended by WMO/WDCGG (Thoning et al., 1989; Masarie and Tans, 1995; WMO, 2000). The values exceeding ±2σ from the fitted curve were excluded. This process was repeated, and σ decreased until all retained points were within ±2σ of the fitted curve. The dataset cleaned this way, now constitutes what we call background data. Afterwards, based on the time series of the retained data, a linear trend was derived first using a least squares method, and then the average seasonal variation of the northern hemispheric CO_2 was derived using a Fourier polynomial with three harmonics based on the maximum entropy spectral analysis (Nakazawa et al., 1991). Subsequently, a long-term trend was obtained by applying a Lanczos filter using a cut-off frequency of 0.48 cycle /year (Duchon, 1979; WMO, 2000). To fill in gaps shorter than 2 months in the observations, a linear interpolation was performed for gaps in the long-term trend, from which the seasonal variation has been subtracted. Subsequently, the time series without any intervals were obtained by adding the average seasonal variation to the interpolated periods.

To understand the contribution of regional or local effects on observed atmospheric greenhouse gases, we analyzed the transport routes of different air masses and then assess the potential source areas which affect CO_2, CH_4 and CO concentrations at stations SDZ and LAN. We computed 3–day backward trajectories coincident with background data and outlier data of CO_2, CH_4 and CO respectively using the Hybrid Single-Particle Lagrangian Integrated Trajectory (HYSPLIT) dispersion model (Draxler and Hess, 1997; Wang, 2009). The starting position of the trajectory was at stations SDZ and LAN, and the height above the surface was 500 m. Therefore, the calculating height of the trajectory corresponds to the middle of the atmospheric boundary layer over these two region; those trajectories are able to reflect the conditions of the mean flow field after diffusion and mixture within the boundary layer. The model is based upon NCEP/NCAR reanalysis data. Five different types of airflow traces were

obtained for stations SDZ and LAN and were used to match the five different kinds of typical air masses.

In this paper, the correlations of ΔCH_4 and ΔCO_2, ΔCO and ΔCO_2, ΔCO and ΔCH_4 were also analyzed by seasons, separately. ΔCO_2, ΔCH_4 and ΔCO denote net changes that can be either higher or lower than background conditions. A relatively large fraction of these net effects is due to regional influences (Akira et al., 2011). We derive our background values from the smooth curves fitted to data at the stations themselves because of the obvious differences in the seasonal cycle between stations (Table 1). The slopes represent mainly the signatures of regional/local emissions (Tohjima et al., 2014). Correlations are calculated using the linear least squares method, accounting for uncertainties in both the x and y directions (Press and Teukolsky, 1992).

3. Results and Discussion

Time series for CO_2, CH_4 and CO mixing ratios at SDZ and LAN are shown in Fig. 2. For station SDZ, the proportions of rejected CO_2, CH_4 and CO measurements are 6.4%, 3.4% and 9.3% (not shown here), the proportions of outliers are 35.0%, 41.9% and 25.3% (red circles), and the proportions of retained measurements are 58.6%, 54.7% and 65.4% (black squares) correspondingly. For station LAN, the proportions of rejected CO_2, CH_4 and CO measurements are 3.4%, 6.5%, and 9.4%, the percentage of outliers are 28.6%, 21.8%, and 33.1%, and the proportions of retained measurements are 68.0%, 71.7%, and 57.5%. The smooth curves for the two stations are shown with blue lines. The difference between background and polluted greenhouse gases time series in these two stations may reflect the possible influence from local and regional sources and sinks.

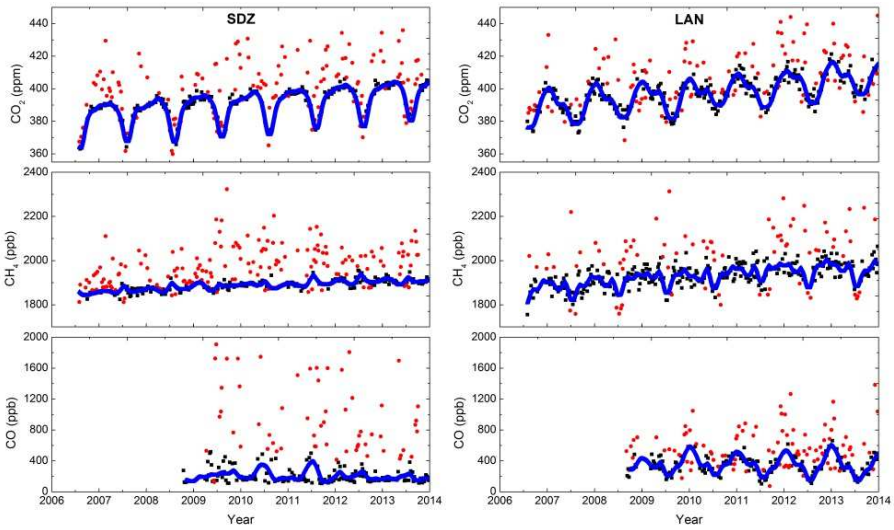

Fig. 2. Time series of atmospheric CO_2 (top), CH_4 (middle) and CO (bottom) mixing ratios observed at SDZ (left) and LAN (right). The red circles are outliers, the black squares are background data, and the blue lines are curve fitted results.

3.1 Trends and seasonal cycle of background CO_2, CH_4 and CO

The background annual means and long-term trends were estimated based on curves fitted to measured CO_2, CH_4 and CO mixing ratios (Fig. 3). Both CO_2 and CH_4 mole fractions at SDZ and LAN show upward trends from 2007 to 2013. At SDZ, the CO_2 annual means vary from 384.3±3.7 ppm to 397.7±3.8 ppm with an average mean growth rate of 2.3±0.2 ppm/yr, while the CH_4 annual means range from 1862.4±8.2 ppb to 1908.3±11.4 ppb with an average mean growth rate of 7.6±1.7 ppb/yr. On the other hand at LAN, the CO_2 annual means fluctuates from 389.9±3.9 ppm to 406.6±3.3 ppm with a mean growth rate of 2.6±0.5 ppm/yr, whereas the CH_4 annual means fluctuates from 1884.4±26.6 ppb to 1958.5±34.0 ppb with a mean growth rate of 11.5±2.9 ppb/yr. Globally, averaged CO_2 and CH_4 in 2013 were 396.0±0.1 ppm and 1824±2 ppb, respectively, while the average growth rate for the past decade was about 2.1 ppm/yr and for CO_2 and 3.8 ppb/yr for CH_4. This suggests a relatively faster increase in the regional greenhouse gases sources in China than the global average.

However, the CO mole fractions at SDZ show a downward trend and the CO annual means vary from 214±29.9 ppb to 178±23.7 ppb in 2009–2013. No apparent upward or downward trend was noticed during the observation period for CO at LAN, and the 5–year annual mean value is 361.8±50.8 ppb.

At the same time, the year-to-year fluctuation changed significantly at LAN. For CO_2, this quantity had a minimum value of 1.5 ppm in 2008–2009, a maximum value of 4.2 ppm in 2011–2012, and a standard deviation of 1.2 ppm; for CH_4, the minimum fluctuation was -1.3 ppb in 2012–2013, the maximum was 24.7 ppb in 2010–2011 and the standard deviation was 10.8 ppb. However, the year-to-year fluctuation changed gradually at SDZ.

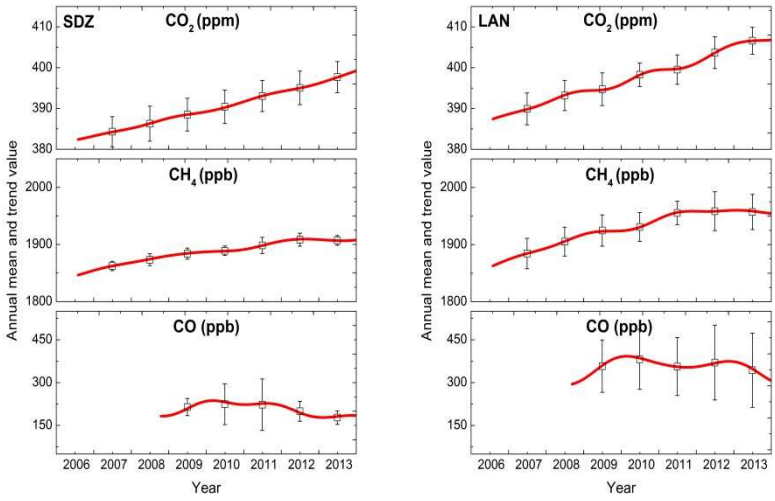

Fig. 3. Annual means (black squares) with uncertainties (error bars) and long-term trends (red lines) for CO_2 (top), CH_4 (middle) and CO (bottom) at SDZ (left) and LAN (right).

In this study, we also compared the results with data from the Tae-ahn Peninsula regional station (TAP) in Korea (36.72°N, 126.12°E, 20 m asl), Ryori regional station (RYO) in Japan (39.03°N, 141.82°E, 260 m asl) and WLG station in China (36.28°N, 100.90°E, 3810 m asl) (http://ds.data.jma.go.jp/gmd/wdcgg/cgi-bin/wdcgg/catalogue.cgi). Fig. 4 shows that the annual means of CO_2, CH_4 and CO at LAN are higher than those measured at other stations from 2007 to 2013. While the values of CO_2 at SDZ are consistent with those obtained at WLG (Zhou et al., 2003) and lower than those measured at the regional stations TAP (Kim et al., 2012, 2014) and RYO (Akira et al., 2011), the CH_4 and CO values are lower than those measured at TAP and higher than those measured at RYO and WLG.

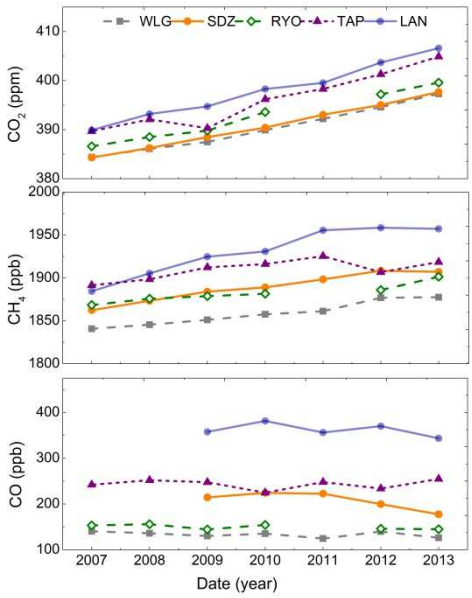

Fig. 4. Estimated atmospheric CO_2, CH_4 and CO annual means at SDZ, LAN and other selected sites, 2007–2013.

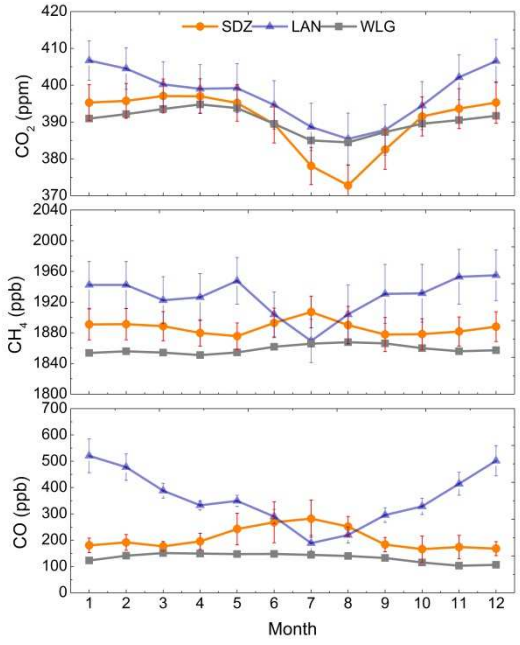

Fig. 5. Seasonal cycles of atmospheric CO_2, CH_4 and CO mixing ratios at SDZ and LAN, the variations are also compared with WLG data, with standard deviations indicated as error bars during the observation period.

Fig. 5 shows the average seasonal cycles of atmospheric CO_2, CH_4 and CO mixing ratios during the observation period at stations SDZ and LAN. For comparison, we also overlay the monthly values from WLG because the seasonal cycles of greenhouse gases at WLG can

show features typical of continental regions at mid- to high northern latitudes that correspond to the seasonal cycle of the terrestrial biosphere (Zhou et al., 2003, 2005; WDCGG, 2014).

Atmospheric CO_2 values reach their minima in August at both SDZ and LAN. However, the maximum appears in January at LAN and in March and April at SDZ. Furthermore, at SDZ, the CO_2 values rapidly decrease from May to August and swiftly increases from August to October. The peak-to-trough seasonal amplitude is 24.3±3.3 ppm. In contrast, at LAN, the changes in CO_2 in the adjacent month are gentler, with peak-to-trough seasonal amplitude of 21.3±2.5 ppm. Particularly notable is that the values of CO_2 are lower in summer and higher in winter at SDZ than at WLG, while the values of CO_2 in summer after removal of the positive outliers at LAN are still greater than those at WLG.

For CH_4, the value at LAN reaches a maximum in December, reaches a second maximum in May, and attains its minimum in July. The maximum and minimum of CO appear in January and July, respectively. However, at SDZ the mean seasonal cycle for CH_4 shows two small peaks in February and July, similar to those observed at WLG. Moreover, the CO data show maxima in July and minima in October.

3.2 Impact analysis of air mass transportation on background CO_2, CH_4 and CO

To understand the contribution of regional effects on background atmospheric GHGs, we analyzed the transport routes (Fig. 6) and got the cluster mean concentrations of CO_2, CH_4, CO corresponding to the 5 cluster air masses at SDZ and LAN (Table 1).

The air masses originate mostly from remote regions of the northwest, north, and northeast, including Russia and Mongolia, in spring, autumn and winter, then pass through Inner Mongolia and the area north of Hebei before arriving at SDZ, except for cluster 3 in spring and autumn. In summer, three clusters (cluster 3, 4, 5) still originate in the north, but the transport distance is shorter; cluster 2 emerges from Hebei province while cluster 1 originates in southeastern Shandong. This indicates that the background CO_2 at SDZ is influenced mainly by clean air masses from remote areas in the spring, autumn, and winter and by terrestrial ecosystems in China in summer but is not influenced by the main urban clusters in JJJ region for example Beijing and Tianjin, during almost the entire year. Therefore, this leads to the observed similarity between SDZ and WLG in terms of the low background

CO_2 mole fraction, similar long-term trends, and lower than that in TAP and RYO as found in Fig. 4. At the same time, in spring, cluster 3 comes from the north, and it is very short, while cluster 4 arises from the northeast of China, it is still in the heating period, so the combustion of fossil fuel and biomass may lead to the higher CO_2 emission in spring than that in winter, and also result in the longer peak period at SDZ in Fig. 5.

In contrast, because LAN is located in the southeastern part of China, the geographic coverage of the trajectories during the four seasons is obviously different from that of SDZ. The air masses first originate mostly from northwest, north and northeast and then pass through northwest-north-central China island areas, for example, clusters 2, 3, 5 in spring, clusters 2, 4, 5 in autumn and winter. Thus, the air masses originating in the north may carry extensive information from man-made sources in the northern parts of China, even including Beijing, which may cause the observed increase in background CO_2 concentrations. At the same time, the carbon uptake by terrestrial ecosystems in the summertime is maybe weakened when the air masses originate from the Southeast China Sea region, so the atmospheric CO_2 concentration is not noticeably reduced. On the other hand, the air masses originating in the Southeast China Sea region will pass Shanghai or Hangzhou with high probability before arriving at LAN, for example cluster 4 and cluster 5 in summer, cluster 1 in spring, and cluster 5 in autumn. So the carbon emissions from large urban clusters in the YRD region may also lead to increase in observed CO_2 concentrations at LAN. Above all, the results can explain the year-round higher background CO_2 mole fraction and the bigger year-to-year fluctuations at LAN, particularly the higher measured values of CO_2 in summer relative to WLG which persist even after positive outliers are removed, because of the stronger influence from anthropogenic activity.

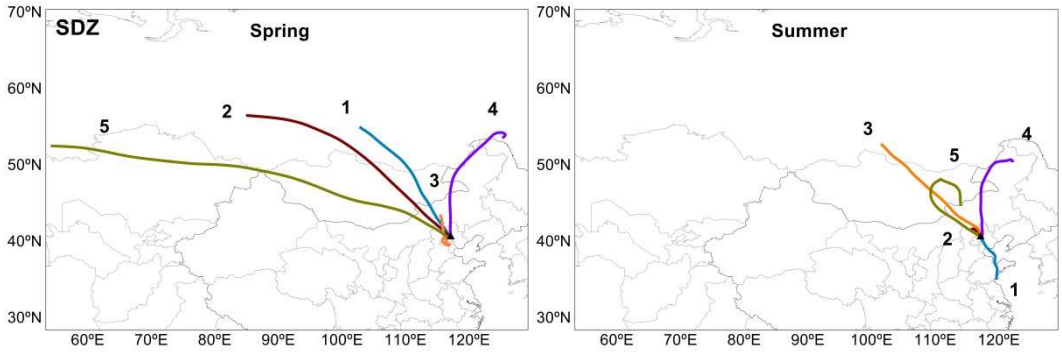

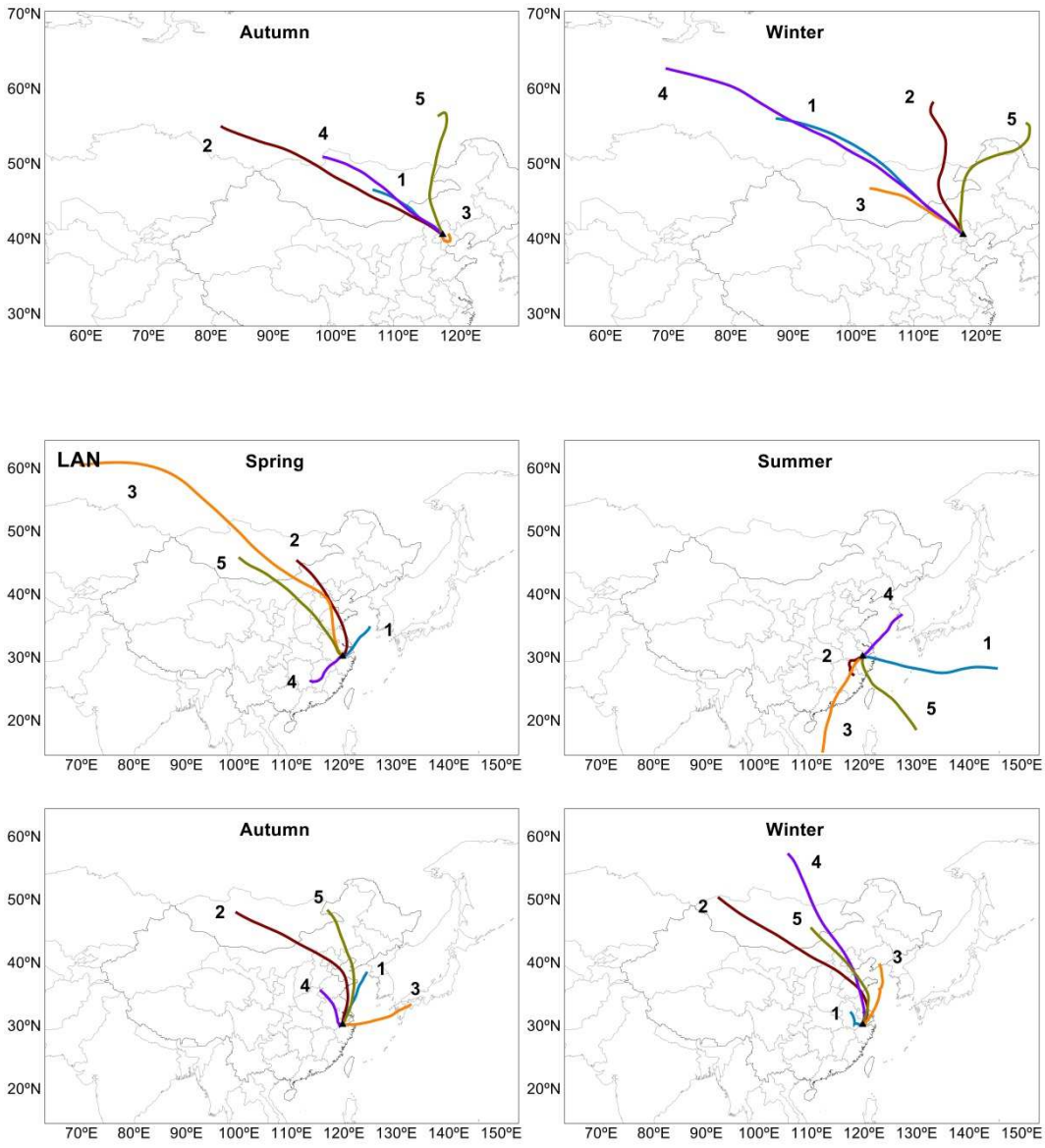

Fig. 6. The cluster means back-trajectories in the four seasons based on the background data at SDZ (top) and LAN (down)**.**

Table 1. The calculated clusters mean concentrations of background CO_2, CH_4 and CO by seasons at SDZ and LAN

	Cluster	SDZ BG						LAN BG					
		CO_2 /ppm		CH_4 /ppb		CO /ppb		CO_2 /ppm		CH_4 /ppb		CO /ppb	
		Share	Mean	Share	Mean	Share	Mean	Share	Mean	Share	Mean	Share	Mean
Spring	1	38.1%	398.6±2.6	37.1%	1889.7±10.8	44.4%	196.5±48.5	49.2%	398.6±6.6	45.5%	1923.6±47.1	52.8%	350.0±70.8
	2	33.3%	396.2±2.8	40.0%	1881.5±12.1	37.0%	154.9±7.8	23.0%	401.0±6.4	25.5%	1922.7±28.3	25.0%	391.5±98.6
	3	7.1%	397.7±5.0	2.5%	1900.4±2.0	3.7%	153.2±3.2	4.9%	402.5±7.3	5.5%	1928.8±9.6	5.6%	295.9±8.5
	4	19.0%	397.2±2.3	17.1%	1883.3±8.0	14.8%	168.2±12.3	13.1%	396.9±10.0	12.7%	1924.0±58.7	8.3%	393.5±80.5
	5	2.4%	390.7±0.3	3.2%	1847.1±1.8	-	-	9.8%	397.0±6.3	10.9%	1919.2±19.2	8.3%	315.5±42.8
	A		397.3±5.0		1884.4±20.2		175.3±61.2		399.0±7.0		1923.2±40.1		358.1±78.0

Summer	1	32.7%	383.6±3.4	38.1%	1916.1±30.0	36.4%	429.1±29.4	4.8%	386.0±3.9	3.0%	1845.0±0.0	2.9%	107.6±0.0
	2	33.9%	376.6±3.2	30.8%	1892.4±17.2	26.4%	275.6±26.4	39.7%	391.3±8.4	39.4%	1914.1±68.8	37.1%	247.9±79.9
	3	4.8%	398.7±0.6	8.1%	1924.5±1.2	9.2%	266.7±2.3	19.0%	387.2±5.3	18.2%	1896.2±48.6	20.0%	207.2±60.8
	4	14.8%	377.0±8.7	15.4%	1883.2±12.0	-	-	22.2%	390.3±8.9	27.3%	1923.4±35.7	20.0%	244.6±47.1
	5	13.8%	385.8±2.5	7.7%	1916.7±1.2	28.0%	145.2±5.7	14.3%	392.7±6.0	12.1%	1873.4±42.5	20.0%	171.6±59.1
	A		381.4±8.8		1904.5±38.5		295.0±124.2		390.2±7.6		1906.4±54.9		219.8±72.2
Autumn	1	23.5%	389.5±3.9	18.0%	1878.3±13.9	24.0%	126.2±11.2	20.7%	393.2±9.4	23.9%	1929.2±40.5	18.4%	344.9±37.4
	2	17.6%	391.8±5.1	20.0%	1882.5±13.2	12.3%	190.4±36.4	20.7%	400.0±4.2	17.4%	1930.9±27.3	13.2%	314.0±83.6
	3	11.8%	386.9±0.8	7.7%	1888.0±12.3	8.0%	165.4±21.3	20.7%	393.0±8.8	21.7%	1926.2±47.9	31.6%	288.0±84.0
	4	35.3%	397.5±3.0	40.0%	1896.7±7.8	43.7%	148.3±14.7	20.7%	401.7±8.1	13.0%	1981.1±48.1	18.4%	393.2±94.1
	5	11.8%	397.4±3.2	14.3%	1902.6±3.7	12.0%	145.6±8.3	20.7%	398.0±9.1	23.9%	1954.7±31.5	18.4%	360.1±36.7
	A		393.4±7.3		1890.4±19.6		149.1±34.4		396.7±8.7		1941.7±42.2		334.6±79.3
Winter	1	27.6%	395.8±3.7	25.9%	1890.8±15.7	20.0%	168.3±12.8	42.6%	406.2±6.2	37.5%	1955.9±37.0	52.6%	491.6±94.7
	2	24.1%	397.2±3.8	18.5%	1909.2±11.3	19.6%	157.4±7.8	13.0%	406.9±8.3	14.6%	1955.2±44.1	10.5%	439.5±52.9
	3	31.0%	398.9±2.7	37.0%	1902.0±11.0	40.1%	181.3±26.3	13.0%	404.6±8.5	14.6%	1933.8±45.2	15.8%	566.1±104.8
	4	10.3%	401.5±1.8	11.1%	1909.4±3.0	15.3%	212.3±54.7	14.8%	403.8±9.4	16.7%	1933.5±29.0	-	-
	5	6.9%	396.4±3.9	7.4%	1896.7±13.8	5.0%	181.7±3.3	16.7%	407.5±5.8	16.7%	1961.1±45.0	21.1%	524.4±37.9
	A		397.7±5.8		1900.8±21.5		178.6±47.6		406.0±7.1		1949.7±39.4		504.8±85.9

CO reaction with OH removes about 75% of the OH from atmosphere, influencing the atmosphere oxidation capacity. Therefore, even small changes in the atmospheric concentration of CO, play an important role in atmospheric chemistry. Particularly in the summer, the photochemical effect is stronger and OH abundance, a dominant sink for atmospheric CH_4 and CO, is also higher, which can lead to the lower levels of CH_4 and CO concentration in summer in the northern hemispheric areas (Thompson, 1992).

As shown in Fig. 6, the length of clusters at SDZ is shorter in summer than those in other seasons. Cluster 2 comes from Hebei province, whereas the transport route of clusters 3, 4 and 5 is in Inner Mongolia. Hebei province is an important region for breeding of cattle and sheep and is adjacent to Inner Mongolia, the largest livestock breeding region in China. Cluster 1 transport by way of Shandong Peninsula and JJJ region, which are important rice producing areas. Therefore, the fact that the seasonal variation in CH_4 includes a summer maximum at SDZ in Fig. 5 suggests that the area is subject to a CH_4 source that is likely due to ruminants as well as air mass transport from the surrounding regions. For CO, cluster 1 in summer passes through the economic urban clusters around the Bohai Sea and JJJ region before arriving at SDZ carried much anthropogenic source of information, so the CO value of cluster 1 is obviously higher than other clusters in summer, which also lead to the higher CO in summer. In contrast, YRD region is the primary rice producing area with much

wetlands and lakes, which lead to the high levels of CH_4 concentration on the whole year at LAN. But, in summer, the photochemical reaction is intense, and the concentration of CH_4 and CO is lower as the sink of OH.

Above all, the background information at SDZ is weakly influenced by local and regional greenhouse gases sources and sinks from JJJ regions, except that in summer, thus providing limited information about anthropogenic emissions in China. Whereas, the background information at LAN station, located in downwind of China, provided some implications of GHGs emissions and uptakes from Northern, Central, and East China. So, the CO_2, CH_4, and CO background values observed at LAN are all higher than other stations.

3.3 Impact analysis of air mass transportation on polluted CO_2, CH_4 and CO

To understand the contribution of regional and local emissions on atmospheric greenhouse gases, we also computed a 3–day backward trajectory coincident with outlier data of CO_2, CH_4 and CO respectively at SDZ and LAN.

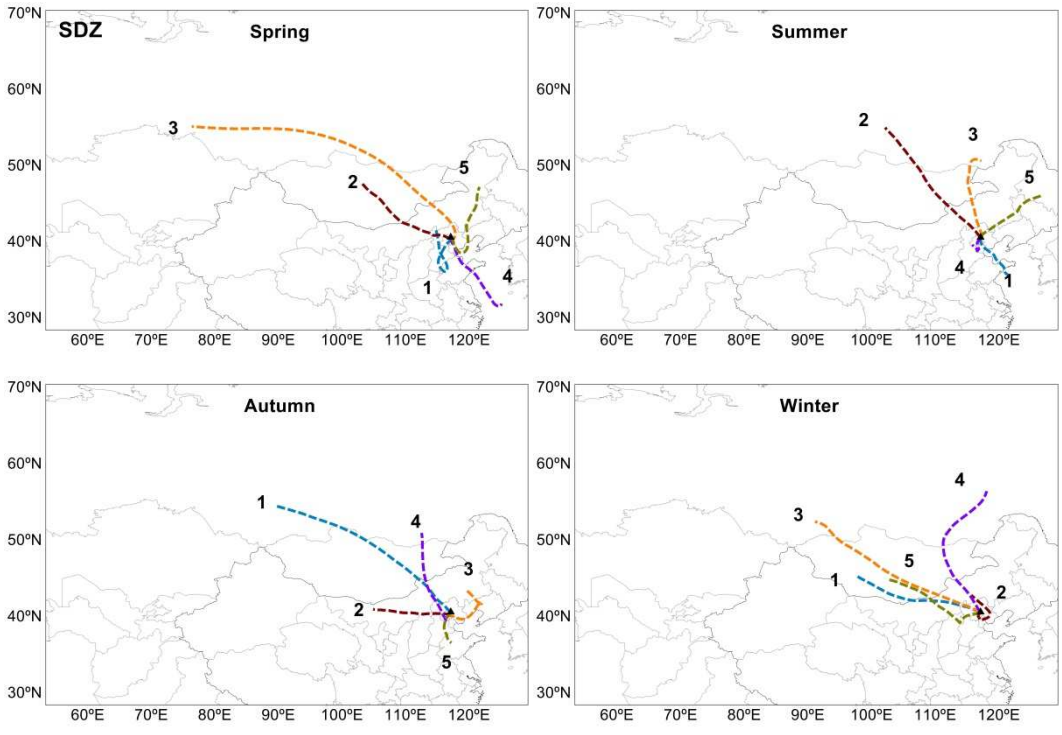

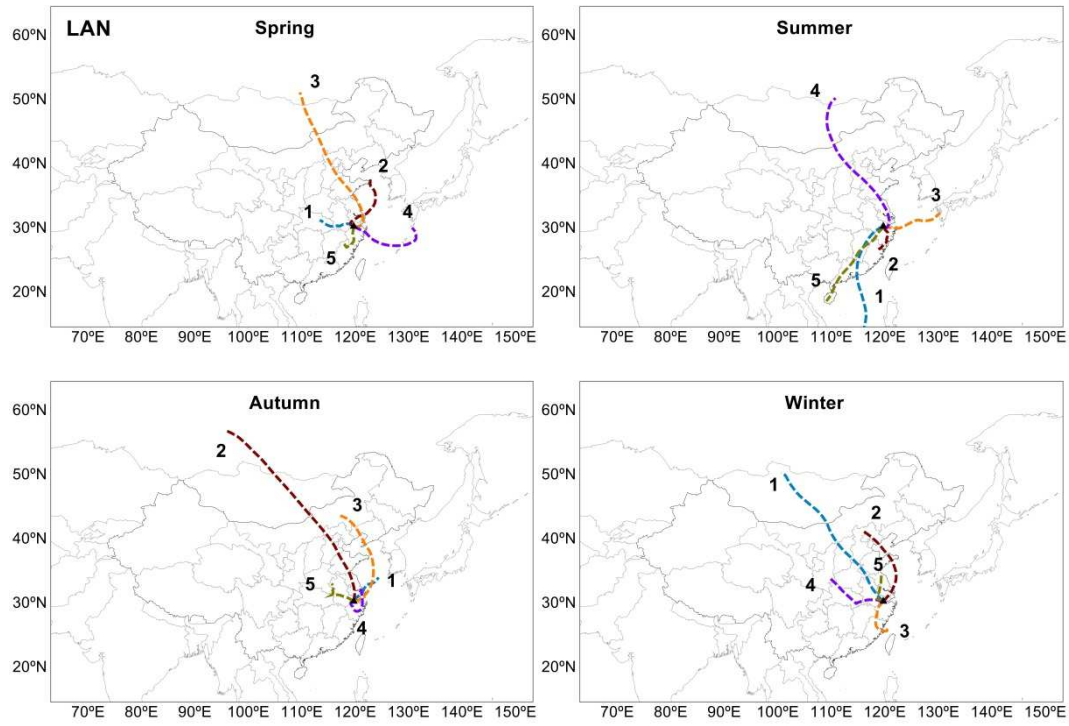

Fig. 7. The cluster means back-trajectories in the four seasons based on the polluted data at SDZ (top) and LAN (down)**.**

Fig. 7 presents that at SDZ, the air masses that come from southwesterly, southerly and southeasterly directions, which is the main gathering area of urban cluster in the JJJ region account for higher proportions. For example, clusters 1, 4, and 5 in spring account for 61.9%, cluster 1 and cluster 4 in summer account for 64%, and cluster 4 and cluster 5 in autumn account for 46.7%. Additionally, cluster 2 and cluster 5 in winter account for 47.8%. Most notably, clusters 1 and 5 in spring, cluster 4 in autumn and cluster 2 and 5 in winter all originate in the north, but they then detour to the south of the JJJ region before reaching SDZ. This means the air data that was defined as the outlier at SDZ are affected strongly by regional and local anthropogenic emissions, which can lead to the higher GHGs concentrations. Similar situations occurred at LAN including clusters 2, 3, and 5 in spring, clusters 2, 3, and 4 in summer, cluster 4 in autumn, and clusters 2 and 5 in winter.

By calculating the clusters' mean concentrations of polluted CO_2, CH_4, and CO corresponding to the 5 clusters' air masses by seasons at SDZ and LAN (Table 2), it was found that the CO_2 concentrations at LAN are still caused by both the influence of the local emission and the long-distance atmosphere transportation in spring and

summer as reflected in section 3.2. For example, the CO_2 concentrations of cluster 3 in spring and cluster 4 in summer are very high because they all ran through the densely populated areas and industrialized areas including Hebei, Shandong and Jiangsu provinces from far and near. At the same time, the carbon uptake by terrestrial ecosystems in the summertime is maybe also weakened when the air masses originate from the Southeast China Sea area, for example clusters 2 and 4 in spring and cluster 3 in summer. In contrast, at SDZ, the CO_2 emissions from heating decrease gradually in spring in the north of China, and then the photosynthesis got stronger from clusters 2, 3, and 5 in summer by the forest and grassland in the north and northeast of China. So, the CO_2 concentration at LAN is higher than that at SDZ in spring and summer.

As the beginning of the heating season in autumn and winter in the north of China, the CO_2 emission from heating increase gradually and in the meanwhile, the CO_2 uptake from photosynthesis decrease, so the CO_2 concentration at SDZ increased accordingly under the prevailing northwesterly winds. However, in the south of China, with the weakening of the air mass transportation from the north during winter, heating is rarely required, and vegetation photosynthesis is still stronger because of the lower latitude. So, the CO_2 concentration at LAN is lower than that at SDZ in autumn and winter.

Table 2. The calculated clusters mean concentrations of polluted CO_2, CH_4 and CO by seasons at SDZ and LAN

		SDZ p							LAN p					
	Cluster	CO_2 /ppm		CH_4 /ppb		CO /ppb			CO_2 /ppm		CH_4 /ppb		CO /ppb	
		Share	Mean	Share	Share	Share	Mean	Share		Share	Mean	Share	Mean	Share
Spring	1	22.8%	405.5±6.4	25.0%	1977.7±54.2	32.0%	1699.0±519.7		28.6%	411.3±20.4	33.3%	2160.4±39.3	27.3%	797.1±88.2
	2	24.3%	408.8±5.1	27.6%	1975.3±41.8	-	-		33.3%	416.1±7.3	-	-	18.2%	625.1±143.4
	3	14.3%	406.0±7.4	10.5%	1970.1±25.7	22.2%	792.0±212.5		9.5%	418.9±2.1	16.7%	2020.4±0.0	18.2%	611.1±12.4
	4	14.7%	424.2±4.0	15.8%	2017.6±9.9	35.0%	1571.7±175.1		9.5%	410.9±21.0	-	-	9.1%	206.5±0.0
	5	23.9%	403.6±3.2	21.1%	1926.1±18.8	10.8%	428.2±60.3		19.0%	413.9±9.2	50.0%	2101.4±125.4	27.3%	471.4±175.1
	A		408.6±10.9		1971.7±67.5		1313.8±713.2			414.1±12.8		2107.6±96.2		589.5±204.7
Summer	1	38.0%	400.8±8.9	41.0%	2050.7±48.5	50.0%	1224.3±279.1		15.0%	395.9±8.2	25.0%	2032.6±264.5	-	-
	2	18.0%	380.0±4.4	15.4%	1890.8±24.4	6.5%	124.8±30.2		30.0%	397.9±9.4	37.5%	2096.7±188.1	25.0%	549.2±0.0
	3	6.0%	376.7±7.2	5.1%	1863.3±16.3	5.0%	145.9±44.5		30.0%	412.0±16.7	12.5%	2247.9±0.0	25.0%	526.9±0.0
	4	26.0%	390.2±8.8	30.8%	2013.4±43.3	28.3%	810.9±236.3		5.0%	416.1±0.0	12.5%	2135.0±0.0	25.0%	737.7±0.0
	5	12.0%	380.5±4.6	7.7%	1974.1±56.7	10.2%	1108.9±259.7		20.0%	392.6±31.9	12.5%	2413.6±0.0	25.0%	481.2±0.0
	A		390.4±16.3		1999.1±98.2		979.8±544.0			401.7±18.4		2144.0±191.2		573.8±112.9
Autumn	1	24.1%	400.8±8.8	19.5%	1989.8±27.2	13.3%	942.3±127.5		19.2%	402.2±9.8	40.0%	2060.3±59.3	21.4%	517.2±56.5

	2	17.2%	418.5±5.5	20.0%	2047.8±18.7	26.7%	1072.8±395.2	11.5%	403.6±16.5	10.0%	2172.0±0.0	7.1%	867.8±0.0
	3	10.3%	408.5±6.8	12.3%	2050.3±31.0	13.3%	774.7±114.5	19.2%	407.0±17.9	30.0%	2073.5±32.3	21.4%	586.8±50.6
	4	20.7%	409.0±4.6	16.0%	2075.9±93.5	20.0%	1007.4±347.3	38.5%	407.0±11.8	20.0%	2165.0±104.7	35.7%	499.2±249.6
	5	27.6%	410.7±5.9	32.2%	2072.0±42.2	26.7%	1089.8±194.4	11.5%	409.0±12.4	-	-	14.3%	553.0±161.7
	A		409.1±12.4		2048.7±84.2		1007.1±457.0		405.9±12.5		2096.4±71.1		555.8±177.1
Winter	1	26.1%	419.3±14.2	26.3%	1957.9±9.5	11.1%	528.8±76.6	12.9%	395.7±6.9	-	-	9.5%	323.7±65.3
	2	26.1%	424.4±7.5	32.1%	2031.6±41.6	45.0%	2614.7±1277.8	22.6%	420.1±16.3	18.2%	2036.1±10.9	19.0%	919.4±117.8
	3	17.4%	407.4±3.0	15.8%	1985.5±22.4	21.7%	500.4±65.8	9.7%	408.8±30.9	9.1%	2157.3±0.0	9.5%	819.8±628.4
	4	8.7%	394.3±0.9	-	-	-	-	16.1%	402.1±16.7	18.2%	2076.6±4.8	14.3%	589.7±399.8
	5	21.7%	417.7±5.6	25.8%	2009.2±42.8	22.2%	1039.8±254.2	38.7%	425.9±15.3	54.5%	2109.7±41.9	47.6%	901.3±298.6
	A		416.0±17.1		1999.0±63.2		1563.1±1746.2		415.2±19.5		2094.6±46.6		797.5±339.8

For atmospheric CH_4 and CO based on outlier data at SDZ and LAN, the main feature is the difference of seasonal change pattern compared with those based on background data. The polluted CH_4 at LAN is obviously higher than the background values for the whole year, and the peak of polluted CH_4 occurs in summer. Fig. 7 shows that the ocean is not the main source of CH_4 during spring, because no air mass with polluted CH_4 was observed in clusters 2 and 4. Similarly, no air mass with polluted CH_4 was observed from the east in autumn and northwest in winter. Overall, the local anthropogenic pollution and the emission from wetlands and rice paddies may lead to the high CH_4 concentration throughout the year. At SDZ, the polluted CH_4 reflects a comprehensive contribution from sources such as rice paddies or wetlands (cluster 5 in summer and cluster 3 in autumn), enteric fermentation (clusters 2, 3 and 4 in autumn and cluster 5 in winter), and fossil fuel combustion (Cluster 4 in spring, clusters 1 and 4 in summer, cluster 5 in autumn, cluster 2 in winter).

For atmospheric CO, it is noteworthy that, the polluted CO values at SDZ is considerably higher than that at LAN, and the CO values in winter and spring are also higher than that in summer and autumn. At the same time, the CO values on different clusters varied considerably except in autumn. For example, in spring, CO in cluster 5 (428.2 ppb), which comes from northeast of China, is far below than cluster 1 (1699.0 ppb), which comes from the JJJ region.

Mass transportation shown in Fig. 7, it can be noticed that the local fossil fuel combustion emission is the main source of CO in spring and summer, while fossil fuel combustion, biomass burning with sheep and cow dung in pasturing areas, and crop stalks in rural areas are the main sources of CO at SDZ. By contrast, the CO value in spring, summer

and autumn at LAN have a little change and is slightly higher in winter due to the transport contribution from JJJ region (cluster 2) and local emission from YRD region.

3.4 Correlation analysis of $\Delta CH_4/\Delta CO_2$, $\Delta CH_4/\Delta CO$ and $\Delta CO/\Delta CO_2$

Although we noticed obvious development on outlier data of CO_2, CH_4, and CO because of the influence from regional transport and urban clusters' emission through backward trajectory analysis, further information about the relationship of the urban clusters emission source with the higher GHGs was still not very clear. In this session, we show the analysis of seasonality in the correlations of ΔCH_4 and ΔCO_2, ΔCO and ΔCO_2, ΔCO and ΔCH_4.

Table 3 shows there is a significant linear relationship between ΔCO_2, ΔCH_4 and ΔCO at SDZ all the year ($p<0.001$), except ΔCH_4-ΔCO_2 in summer. But no correlativity is observed in summer and autumn among ΔCO_2, ΔCH_4, and ΔCO and ΔCO-ΔCH_4 in winter at LAN. This result indicates that the enhanced values of CO_2, CH_4 and CO all share the common-source of anthropogenic emissions from the regional fossil fuel and biomass burning in cold seasons (spring and winter) at SDZ and LAN.

In YRD region, the photochemical reaction is very pronounced with abundant OH under the high temperature and humidity climate in summer and autumn, which results in a dominant sink for atmospheric CH_4 and CO. At the same time, large quantities of CH_4 were released to the atmosphere from vast rice paddies and wetlands there. Therefore, the combined effect of different sources and sinks of CO_2, CH_4, and CO lead to irrelevance among them.

However, although the photochemical reaction still exists in warm season in the JJJ region, the weaker reaction leads to a weaker sink for CH_4 and CO than that in YRD region. Secondly, wetlands and rice paddies are not the primary sources for CH_4 in the north of China because of drought and water shortage, especially in northwest and North China. Thirdly, the proportion of straw burning in the north is higher than that in the south. These are why the correlativity among CO_2, CH_4 and CO in summer and autumn is still significant at SDZ.

Table 3. The relationship of ΔCO_2, ΔCH_4 ΔCO by seasons.

Seasons	SDZ		LAN	
	Slope (ppm/ppm)	R^2	Slope (ppm/ppm)	R^2

Spring	$\Delta CH_4/\Delta CO_2$	5.81±0.47	0.644	4.09±0.21	0.730
	$\Delta CO/\Delta CO_2$	**55.42±6.40**	0.583	14.07±1.34	0.664
	$\Delta CO/\Delta CH_4$	7.19±0.89	0.544	1.62±0.18	0.604
Summer	$\Delta CH_4/\Delta CO_2$				
	$\Delta CO/\Delta CO_2$	**33.23±3.77**	0.583		
	$\Delta CO/\Delta CH_4$	4.09±0.38	0.671		
Autumn	$\Delta CH_4/\Delta CO_2$	6.84±0.47	0.701		
	$\Delta CO/\Delta CO_2$	**38.38±1.79**	0.893		
	$\Delta CO/\Delta CH_4$	3.99±0.35	0.689		
Winter	$\Delta CH_4/\Delta CO_2$	5.17±0.14	0.944	4.15±0.40	0.546
	$\Delta CO/\Delta CO_2$	**60.22±8.05**	0.529	20.05±1.40	0.794
	$\Delta CO/\Delta CH_4$	12.52±1.42	0.621		

It is worth mentioning that, the $\Delta CO/\Delta CO_2$ correlation slope in spring and winter at SDZ is obviously higher than that in summer and autumn, and considerably greater than that in spring and winter at LAN.

CO is co-emitted with CO_2 from combustion sources, leading to a significant positive correlation between them when combustion is a significant source of observed CO_2. The higher $\Delta CO/\Delta CO_2$ slope in cold season at SDZ means the combustion efficiency is very low than that in summer and autumn. In a previous study (Cao, 2005), straw and firewood burning were main emission sources, and the regions with higher discharged amounts of the pollutants per unit area distributed in a belt shape across the main places of agricultural production of China, from north-east to middle-south. In the north of China, biomass burning including crop stalks in rural areas and sheep and cow dung in pasturing area for heating, and the regular burning stalks in early winter after harvesting and spring before sowing (Liu, 2011; Wang, 2016), which has low combustion efficiency compared to most other fossil energy uses, is still popular. In 2007, the CO emission in JJJ and YRZ was 4620 and 4863 kt (lack of data in Shanghai), respectively. However, the CO emissions in other regions of north, for example, Heilongjiang, Jilin, Liaoning, Inner Mongolia, Shandong, Shanxi, was 4338, 2487, 2918, 1169, 5429, 4338 kt, respectively (Lu, 2011), and the air masses originate from these regions has important effects on the higher CO_2 and CO concentrations at SDZ. This introduces not only the serious regional air pollution, but also the higher $\Delta CO/\Delta CO_2$ slope in our study.

Table 4. Fossil fuel consumption in standard coal equivalent in JJJ and YRD region, 2007–2013.

Region	Energy	2012	2011	2010	2009	2008	2007
JJJ	Coal (%)	74.3%	74.3%	74.0%	75.9%	75.8%	77.0%
	Petroleum (%)	21.2%	22.0%	22.2%	20.5%	20.9%	20.4%
	Natural Gas (%)	4.6%	3.7%	3.8%	3.6%	3.3%	2.6%
	Total (10^4 tce)	49618	48884	44442	40670	38258	36936
	Per unit area (tce/km^2)	2273	2239	2036	1863	1752	1692
YRD	Coal (%)	62.3%	63.0%	61.4%	62.1%	63.2%	63.4%
	Petroleum (%)	32.9%	32.8%	35.1%	34.9%	33.8%	34.0%
	Natural Gas (%)	4.9%	4.2%	3.5%	3.0%	3.0%	2.5%
	Total (10^4 tce)	61574	61410	56017	50867	49116	47547
	Per unit area (tce/km^2)	2891	2883	2630	2388	2306	2232

In the warm seasons, although the above activities of biomass burning reduced, the pattern of development in the JJJ region has focused on heavy industry, equipment manufacture and high-tech industries; therefore, the problems associated with high energy consumption are very prominent there (Guo et al., 2012; Liu et al., 2010; Wu et al., 2014), especially coal occupies large proportion. On the other hand, the YRD region is the most important economic center in China. As a global manufacturing center, it also accounts for a substantial proportion of China's energy consumption. Table 4 summarized the fossil fuel consumption situation in the two regions (http://data.stats.gov.cn/). It is found that coal in the proportion of primary energy consumption in JJJ region is far above than in YRD region. Taking in consideration the low CO_2 emission factor (the CO_2 emission factors for coal, petroleum, and natural gas are 2.408 t/t, 3.065 t/t, and 21.840 10^{-4}t/m^3, respectively) (IPCC, 2006; http://free.xiaze.com/nianjian/zgnytjnj2013/), this may lead to the stronger correlation and higher slope values of ΔCO and ΔCO_2 at SDZ.

4. Conclusions

The low background CO_2 mole fraction was observed at SDZ because most of the air masses originate mostly from remote clean terrestrial areas in the north with limited information of anthropogenic emissions. But the background CH_4 and CO is much higher in summer as influenced by the surrounding regions and urban clusters emission in the JJJ region. Whereas, the CO_2, CH_4 and CO background values observed at LAN are higher due to the combined effects of long-distance transportation from Northern and Central China and urban clusters emission from YRD region.

The polluted GHGs concentration is higher compared to the background data at both

SDZ and LAN as affected by the regional and local anthropogenic emissions. On the other hand, the CO_2 concentration at LAN is lower than that at SDZ in autumn and winter because of the weaken air mass transportation from the north and no heat generation is needed in winter while vegetation photosynthesis is still stronger in the south of China. Additionally, the polluted CO value at SDZ was found considerably higher than that at LAN, especially in spring and winter.

The significant correlation between ΔCO_2-ΔCO ΔCO_2-ΔCH_4 and ΔCH_4-ΔCO was found at the two stations, which means they may share the common-source of anthropogenic emissions from the regional fossil fuel and biomass burning in cold season. Moreover, the high coal-consumption proportion with the low CO_2 emissions factors, and much biomass burning with low combustion efficiency in JJJ region lead to the higher slope values of ΔCO_2 and ΔCO in spring and winter at SDZ and considerably higher than that at LAN.

The results from this study can lay the foundation for more profound studies on atmospheric GHGs level of different areas in China and could be used to improve the understanding of carbon source and sink distribution. Nonetheless, due to the limitation of lower sampling frequency, we cannot carry out the clusters correlation analysis among ΔCO_2, ΔCH_4 and ΔCO and the potential source analysis. Due to the lack of monthly or quarterly data on fossil fuel and biomass combustion, the contribution of regional anthropogenic sources has not been well studied. To better understand and identify a specific source or sink and its exchanging processes in urban clusters, more intensive observation in typical regions for example the Pearl River Delta are also needed.

Acknowledgments

We thank the staff at SDZ, LAN and WLG for collecting flask air samples. This work was supported by the International S&T Cooperation Program of the MOST (No. 2015DFG21960) and the National Natural Science Foundation of China (No. 40905066, 41175116, 41273097 and 41303052). We also thank Tae-ahn in Korea and Ryori in Japan for providing CO_2, CH_4 and CO monthly data from 2007 to 2013. The monthly data are downloaded from World Data Centre for Greenhouse Gases (WDCGG). We thank NOAA

ESRL for hosting Lixin Liu as a visiting scientist. We also greatly appreciate NOAA ESRL for long-term cooperation in flask air sampling program and Ken Masarie for helping us with the data processing.

References

Akira, W., Hidekazu, M., Yousuke, S. et al., 2011. Seasonal variation of enhancement ratios of trace gases observed over 10 years in the western North Pacific. Atmos. Environ. 45 (12), 2129–2137.

Boden, T.A., Marland, G., Andres, R.J., 2010. Global, regional and national fossil-fuel CO_2 emissions, in Trends: A Compendium of Data on Global Change, Carbon Dioxide Inf. Anal. Cent., Oak Ridge Natl. Lab., U.S. Dep. of Energy, Oak Ridge, Tenn., http://cdiac.ornl. gov/trends/emis/overview.html.

Cao G.L., Zhang X.Y., Wang D., et al., 2005. Inventory of Atmospheric Pollutants Discharged from Biomass Burning in China Continent. China Environ. Sci. 25(4): 389-393.

Deng, J.X., Liu, X., Wang, Z., 2014. Characteristics Analysis and Factor Decomposition Based on the Regional Difference Changes in China's CO_2 Emission. J. Nat. Res. 29(2), 189–200.

Draxler, R.R., Hess, G.D., 1997. Description of the HYSPLIT24 Modeling System. NOAA Technical Memorandum, ERL ARL-224.

Duchon, C.E., 1979. Lanczos Filtering in One and Two Dimensions. J. Appl. Meteor.18, 1016–1022.

Du, Y., Fan, J., 2008. Research on Spatial Function Diversity of Metropolitan Economic Regions Based on "Industries & Population" Agglomeration Analysis: Illustrations from Chinese "Three Large Metropolitan Economic Region". Acta Sci. Natur. Univ. 44(3), 467–474.

Fang, S.X., Zhou, L.X., Masarie, K.A., Xu, L, Rella, C.W., 2013. Study of atmospheric CH_4 mole fractions at three WMO/GAW stations in China. J. Geophys. Res. -Atmos. 118, 1–13, doi:10.1002/jgrd.50284.

Fang, S.X., Zhou, L.X., Tans, P.P., Ciais, P., Steinbacher, M., Xu, L., Luan, T., 2014. In situ measurement of atmospheric CO_2 at the four WMO/GAW stations in China. Atmos. Chem. Phys. 14, 2541–2554. Doi: 10.5194/acp–14–2541–2014.

Feng, Z.M., Yang, L., Yang, Y.Z., You, Z., 2013. The Process of Population Agglomeration/Shrinking and Changes in Spatial Pattern in the Beijing-Tianjin-Hebei Metropolitan Region. J. Geoinform. Sci. 15(1), 11–18.

Gamnitzer, U., Karstens, U., Kromer, B., Neubert, R.E.M., Meijer, H.A.J., Schroeder, H., Levin, I., 2006. Carbon monoxide: A quantitative tracer for fossil fuel CO_2? J. Geophys. Res.-Atmos. 111, D22302, doi: 10.1029/2005jd006966.

Gregg, J.S., Andres, R.J., Marland, G., 2008. China: Emissions pattern of the world leader in CO_2 emissions from fossil fuel consumption and cement production. Geophys. Res. Lett. 35, L08806, doi: 10.1029/ 2007GL032887.

Guo J., Zhang Z., Meng L., 2012. China's provincial CO_2 emissions embodied in international and interprovincial trade. Energy Policy. 42, 486–497.

Han S., Kondo, K., Oshima, N., Takegawa, N., Miyazaki, Y., Hu, M., Lin, P., Deng, Z., Zhao, Y., Sugimoto, N., Wu, Y., 2009. Temporal variations of elemental carbon in Beijing. J. Geophys. Res. 114, D23202, doi: 10.1029/2009JD012027.

IPCC 2006, 2006 IPCC Guidelines for National Greenhouse Gas Inventories, Prepared by the National Greenhouse Gas Inventories Programme, Eggleston H.S., Buendia L., Miwa K., Ngara T., and Tanabe K. (eds). Published: IGES, Japan.

Kim, H.S., Chung, Y.S., Kim, J.T., 2014. Spatio-temporal variations of optical properties of aerosols in East Asia measured by MODIS and relation to the ground-based mass concentrations observed in Central Korea during 2001–2010. Asia Pac. J. Atmos. Sci. 50, 191–200.

Kim, H.S., Chung, Y.S., Lee, S.G., 2012. Characteristics of aerosol types during large-scale transport of air pollution over the Yellow Sea region and at Cheongwon, Korea, in 2008. Environ. Monit. Assess. 184, 1973–1984.

Lang, P.M., Dlugokencky, E.J., Masarie, K.A., et al., 1994. Atmospheric methane data for 1989–1992 from the NOAA/CMDL global cooperative air sampling network, NOAA Tech. Memo. ERL CMDL-7, NOAA Environ. Res. Lab., Boulder, Colo.

Levin, I., Karstens, U., 2007. Inferring high-resolution fossil fuel CO_2 records at continental sites from combined $^{14}CO_2$ and CO observations. Tellus, Ser. B. 59, 245–250, doi:10.1111/j.1600–0889.2006.00244.x.

LU B., KONG S.F., HAN B., et al., 2011. Inventory of atmospheric pollutants discharged from biomass burning in China continent in 2007. China Environ. Sci. 31(2): 186-194

Liu L.X., Zhou L.X., Vaughn, B., Miller, J.B., et al., 2014. Background variations of atmospheric CO_2 and carbon-stable isotopes at Waliguan and Shangdianzi stations in China. J. Geophys. Res. Atmos. 119, 5602–5612, doi:10.1002/2013JD019605.

Liu, L.X., Zhou, L.X., Zhang, X.C., Wen, Y.P., Zhang, F., Yao, B., Fang, S.X., 2009. The characteristics of atmospheric CO_2 concentration variation of four national background stations in China. Sci. China Ser. D-Earth Sci. 52(11), 1857–1863, doi: 10.1007/s11430–009–0143–7.

Liu Z., 2015. “China’s Carbon Emissions Report 2015.” Sustainability Science Program and Energy Technology Innovation Policy research group, Belfer Center Discussion Paper #2015–02. Harvard Kennedy School of Government, Cambridge, MA.

Liu, Z.C., Wang, A.J., Yu, W.J., et al., 2010. Research on Regional Carbon Emissions in China. ActaGeosci. Sin. 31(5), 727–732.

Long, R., Shao, T., 2015. Difference in carbon productivity among China's three economic circles and influencing factors. Res. Sci. 37(6), 1249–1257.

Masarie, K.A., Tans, P.P., 1995. Extension and integration of atmospheric carbon dioxide data into a globally consistent measurement record. J. Geophys. Res. 100(D6), 11593–11610.

Nakazawa, T., Miyashita, K., Aoki, S., Tanaka, M., 1991. Temporal and spatial variations of upper tropospheric and lower stratospheric carbon dioxide. Tellus, Ser. B. 43, 106–117.

Press, W.H., Teukolsky, S., 1992. Fitting straight line data with errors in both coordinates. Comput. Phys. 6(3), 274–276.

Pu, J.J., Xu, H.H., He, J., Fang, S.X., Zhou, L.X., 2014. Estimation of regional background concentration of CO_2 at Lin'an Station in Yangtze River Delta, China. Atmos. Environ. 94, 402–408.

Sun, W., Wu, R.H., 2012. Study on the balance of carbon budget and its spatial differentiation in Yangtze River Delta. Geograp. Res. 31(12), 2220–2228.

Thompson, A. M., 1992. The oxidizing capacity of the Earth's atmosphere: Probable past and future changes, Science. 256, 1157-1168.

Thoning, K.W., Tans, P. P., Komhyr, W. D., 1989. Atmospheric carbon dioxide at Mauna Loa Observatory Analysis of the NOAA GMCC data, 1974–1985. J. Geophys. Res. 94, 8549–8565.

Tohjima, Y., Kubo, M., Minejima, C., et al., 2014. Temporal changes in the emissions of CH_4 and CO from China estimated from CH_4/CO_2 and CO/CO_2 correlation observed at Hateruma Island. Atmos. Chem. Phys. 14, 1663–1677.

Trolier, M., White, J.W.C., Tans, P.P., Masarie, K.A., Gemery, P.A., 1996. Monitoring the isotopic composition of atmospheric CO_2: Measurements from the NOAA Global Air Sampling Network. J. Geophys. Res. 101(D20), 25897–25916.

Turnbull, J.C., Miller, J.B., Lehman, S.J., Tans, P.P., Sparks, R.J., Southon, J., 2006. Comparison of (CO_2)-C14, CO, and SF_6 as tracers for recently added fossil fuel CO_2 in the atmosphere and implications for biological CO_2 exchange. Geophys. Res. Lett. 33, L01817, doi: 10.1029/2005GL024213.

Wang T.T., Chen L.F., Tao J.H., et al., 2016. The study of the effects on carbon monoxide in Northeast China from Biomass burning. Remote Sensing Tech. and Application. 31(2): 297-306.

Wang, Y.Q., Zhang, X.Y. and Draxler, R., 2009. TrajStat: GIS-based software that uses various trajectory statistical analysis methods to identify potential sources from long-term air pollution measurement data. Environmental Modelling & Software, 24: 938-939.

Wang, Y.S., Zhang, J.K., Wang, L.L., Hu, B., Tang, G.Q., Liu, Z.R., Sun, Y. Ji, D.S., 2014. Researching significance, status and expectation of haze in Beijing-Tianjin-Hebei region. Adv. Earth Sci. 29(3), 388–396.

WMO, 2009. 15th WMO/IAEA Meeting of Experts on Carbon Dioxide Concentration and Related Tracers Measurement Techniques, No. 194, Jena, Germany.

WMO, 2011. 16th WMO/IAEA Meeting of Experts on Carbon Dioxide Concentration and Related Tracers Measurement Techniques, No. 206, Wellington, New Zealand.

WMO, 2000. WMO World Data Centre for Greenhouse Gases (WDCGG) Data Summary: Volume IV – Greenhouse Gases and Other Atmospheric Gases, No. 22, Japan Meteorological Agency in co-operation with World Meteorological Organization, March 2000. (http://ds.data.jma.go.jp/gmd/wdcgg/pub/products/summary/sum22/sum22.pdf)

WMO, 2014. WMO World Data Centre for Greenhouse Gases (WDCGG) Data Summary: Volume IV – Greenhouse Gases and Other Atmospheric Gases, No. 38, Japan Meteorological Agency in co-operation with World Meteorological Organization, March 2014. (http://ds.data.jma.go.jp/gmd/wdcgg/pub/products/summary/sum38/sum38.pdf)

World Meteorological Organization (WMO), 2015. WMO greenhouse gas bulletin: The state of greenhouse gases in the atmosphere based on global observations through 2014. Geneva.

Wu, H.M., Huang, A.N., Huang, X.X., 2012. Variation Characteristics of Seasons in the Yangtze River Delta during the Past 50 Years Past 50 Years. Chinese J. Agrometeor.

33(3), 317–324.
Wu, Y.Q., Zhao, Y.N., 2014. Beijing-Tianjin-Hebei Energy consumption, carbon emission and economic growth. Econo. Manag. 28(2), 5–12.
Zang, K.P., Zhou, L.X., Fang, S.X., Wen, Y.P., Yao, B., Zhang, F., Liu, L.X., 2011. A new system for calibration and propagation of mixed CO_2 and CH_4 standards. Environ. Chem. 30 (2), 511–516.
Zhang, F., Zhou, L.X., Novelli, P.C., Worthy, D.E.J., et al., 2011. Evaluation of in situ measurements of atmospheric carbon monoxide at Mount Waliguan, China. Atmos. Chem. Phys. 11, 5195–5206.
Zhang, F., Zhou, L.X., 2013a. Implications for CO_2 emissions and sinks changes in western China during 1995–2008 from atmospheric CO_2 at Waliguan, Tellus, Ser. B. 65, 19576, http://dx.doi.org/10.3402/tellusb.v65i0.19576.
Zhang, F., Zhou, L.X., Xu, L., 2013b. Temporal variation of atmospheric CH_4 and the potential source regions at Waliguan, China. Sci. China Ser. D-Earth Sci. 56(5), 727–736.
Zhang, X.C, Cai, Y.X, Wen, Y.P., et al., 2005. Study of atmospheric carbon dioxide calibration and flask sample analysis system. Meteorol. Sci. Technol. 33(6), 538–547.
Zhao, C.L., Tans, P.P., Thoning, K.W., 1997. A manometric system for absolute calibrations of CO_2 in dry air. J. Geophys. Res.102 (D5), 5885–5894.
Zhou, L.X., Conway, T.J., White, J.W.C., et al., 2005. Long-term record of atmospheric CO_2 and stable isotopic ratios at Waliguan Observatory: Background features and possible drivers, 1991–2002. Global Biogeochem. Cycles, 19, GB3021, doi: 10. 1029/2004GB002430.
Zhou, L. X., D. Kitzis, P. P. Tans, “Report of the fourth WMO round-robin reference gas intercomparison, 2002–2007” in the report of the 14th WMO/IAEA meeting of experts on carbon dioxide, other greenhouse gases and related tracers measurement techniques, Helsinki, Finland, 10–13 September 2007, edited by T. Laurila, WMO/GAW Report No. 186, 2009.
Zhou, L.X., Liu, L.X., Zhang, X.C., et al., 2008. Preliminary Results on Network Observation of Greenhouse Gases at China GAW Stations. J. Appli. Meteor. Sci. 19(6), 641–645.
Zhou, L.X., Tang, J., Wen, Y.P., et al., 2003. The impact of local winds and long-range transport on the continuous carbon dioxide record at Mount Waliguan, China. Tellus, Ser. B. 55, 145–158.
Zhou, L.X., Wen, Y.P., Li, J.L., et al., 2004a. Background variation in atmospheric carbon monoxide at Mt. Waliguan, China. ActaScien. Circum. 24(4), 637–642.
Zhou, L.X., Worthy, D.E.J., Lang, P.M., et al., 2004b. Ten years of atmospheric methane observations at a high elevation site in Western China. Atmos. Environ. 38, 7041–7054.